Submitted for the 12th Conf. on Aviation, Range, and Aerospace Meteor. 29 Jan. – 2 Feb. 2006. Atlanta, GA.

P1.9 GAP-FILLING IN 3D RADAR MOSAIC ANALYSIS USING VERTICAL PROFILE OF REFLECTIVITY

Jian Zhang[1], Carrie Langston[1], Kenneth Howard[2], and Beth Clarke[1]

[1]Cooperative Institute for Mesoscale Meteorological Studies, The University of Oklahoma, and
[1,2] NOAA/OAR National Severe Storms Laboratory, Norman, OK

1 INTRODUCTION

Three-dimensional (3-D) radar reflectivity data has become increasingly important data sources for convective scale numerical weather predictions (NWP). Because of the high spatial and temporal resolution of radar data towards depicting important meteorological features, their usage in data assimilation has increased over the recent years. Typically, reflectivity data are objectively analyzed onto 3-D Cartesian grid prior to being assimilated into the atmospheric models. Due to the earth's curvature and positive scan elevation angles, the height of the lowest radar beam increases as range increases from the radar location. As a result, data voids exist below the lowest radar beams when volume scans of radar data are transformed onto a 3-D Cartesian grid. Figure 1 shows radar beam propagation paths under standard refraction conditions. The bottom of the 0.5° tilt is ~1.5 (4) km above the radar at 150 (250) km of range. Since many areas in the conterminous United States (CONUS) are farther than 150km away from the nearest radar (Fig. 2), there exists data voids below 1.5km (or even higher if radar is located on mountain top or the 0.5° tilt is blocked) above mean sea level in those areas. These data voids result in discontinuities in reflectivity analysis fields and pose a problem for accurate depiction of atmospheric processes for data assimilation.

The data voids in radar observations can also impact the accuracy of precipitation estimations derived from radar due to non-uniform vertical profiles of reflectivity (VPR). Many studies have shown improvements to radar precipitation estimations with the application of VPR corrections. It was found that errors in radar-based rainfall estimation due to non-uniform VPR were as significant as the errors in the Z-R and Z-S relationships for winter precipitation (Zawaziki 1984; Joss and Waldvolgel 1990). To correct for the errors due to non-uniform VPR, Koistinen (1991) estimated mean daily VPR at close ranges and applied it at far ranges for the radar rainfall estimations. Seo et al. (2000) developed a real-time technique to adjust range-dependent bias in the WSR-88D rainfall estimates due to non-uniform VPR. The range correction algorithm was evaluated for a Pacific Northwest winter storm using rain gage data. It was found that the range correction technique had potential of significantly improving WSR-88D rainfall estimates for large-scale stratiform precipitation, especially with complex terrain. Pellarin et al. (2002) assessed hydrological impact of the space-time structure of the radar rain-rates error resulted from VPR among others using two S-band weather radars in France. Berne et al. (2004) investigated VPR correction using gauge and vertical pointed radar observations. The current study examines 3-D reflectivity structure associated with specific weather regimes. From these segregated regimes, VPRs are derived using reflectivity observations at the close ranges to obtain accurate depiction of the vertical structure for specific weather regimes (stratiform and convective). Then at the far ranges, the regime specific VPRs are used to extrapolate reflectivity from the lowest radar tilt down to the surface. The extrapolation effectively fills in the gaps at lower levels in the 3D reflectivity grid with the similar weather regimes. Preliminary results from a convective and a stratiform VPRs are presented in this paper.

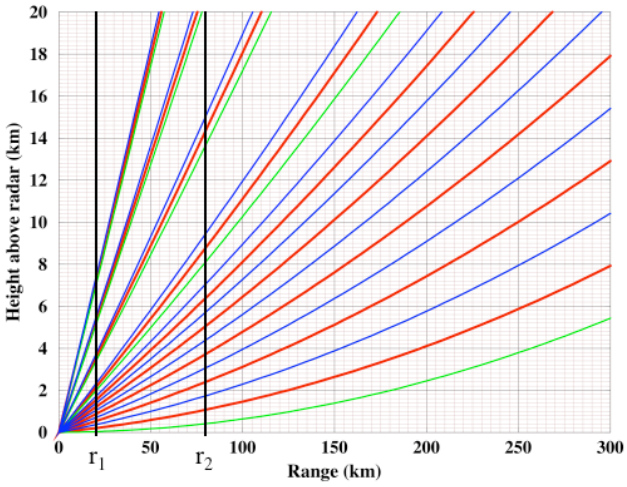

Fig. 1 WSR-88D beam propagation path (VCP21) under standard atmospheric refractive conditions. The bold black vertical lines indicate the ranges between which volume scan reflectivity data are used to derive vertical profiles of reflectivity.

*Corresponding Author address: Jian Zhang, 1313 Halley Circle, Norman, OK 73069; e-mail: jian.zhang@noaa.gov.

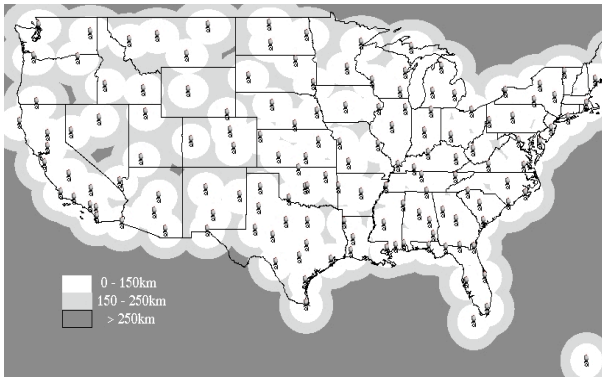

Fig. 2 Distance (km) from anywhere in the contiguous United States to the nearest radar.

Section 2 describes methodology of VPR calculations and case study results of the VPR characteristics of different precipitation types (convective and stratiform). Section 3 presents case study results of gap filling in the 3D reflectivity mosaic using VPR. The last section, section 4, provides a summary.

2 Convective/stratiform VPR

2.1 Methodology

To compare and contrast the advantageous of deriving VPRs specific to weather regimes, two methodologies of VPR are investigated:

1) Volume mean VPR

Within the first methodology, one mean VPR is derived for each volume scan. A volume scan of reflectivity data are first quality controlled to remove non-precipitation echoes. Then the reflectivity observations in an annular region between two pre-specified ranges (r_1 and r_2, Fig. 1) on all tilts are grouped according to heights of the observations (at the center of the radar bins) into evenly spaced vertical layers with a thickness of Δh (default = 200m). The number of layers, N, is determined by two pre-specified height parameters, h_0 and h_t (default = 0.5 and 20km above radar level, respectively), which represent the bottom and top of the domain where VPR is to be derived. The height of each vertical layer, h[k], are defined as the following:

$$N = (h_t - h_0)/\Delta h + 1 \quad (1)$$

$$h[k] = h_0 + k*\Delta h; \quad k = 0, N-1 \quad (2)$$

Here k is the layer index. Within each layer the mean and standard deviation of all the reflectivity observations are computed as following:

$$\bar{Z}[k] = \frac{1}{M}\sum_{i=1}^{M} Z[i]; \qquad k = 0, N-1. \quad (3)$$

$$\sigma_{Z[k]} = \frac{1}{M}\sqrt{\sum_{i=1}^{M}\left(Z[i] - \bar{Z}\right)^2}; \quad k = 0, N-1. \quad (4)$$

Here $\bar{Z}[k]$ is the mean reflectivity in the k^{th} layer and $\sigma_{Z[k]}$ is the standard deviation, M is total number of reflectivity observations in the k^{th} layer, i is the index of reflectivity observations, and Z[i] is an observed reflectivity value within the k^{th} layer. A reflectivity bin is considered to be in the k^{th} layer if:

$$h[k] - 0.5*\Delta h \le h_Z[i] \le h[k] + 0.5*\Delta h; \quad (5)$$

where $h_Z[i]$ is the height at the center of the reflectivity bin.

Two rules are applied to assure a representative and robust VPR: i) only reflectivities higher than a threshold (Z_0) are included in VPR, and ii) a minimum number (M_0) of reflectivity observations with $Z[i] \ge Z_0$ are required within each height layer to get a valid mean reflectivity for the VPR. Both Z_0 and M_0 are adaptable parameters (default = 10 dBZ and 10, respectively). If at any given layer a valid $\bar{Z}[k]$ cannot be obtained, then a linear interpolation using valid $\bar{Z}$ values from layers above and below is performed to get an alternative $\bar{Z}[k]$. The searching radius for valid $\bar{Z}$ values is limited within Δh_{intp} = ± 1km (adaptable). A running 3-point smoother is applied to the final VPR to reduce random fluctuations.

2) Convective/stratiform VPR

Within the second methodology, two VPR are derived for each volume scan, one for convective and one for stratiform echoes. Each vertical column (in the spherical coordinates) in the volume scan data are analyzed and classified as either being convective or stratiform precipitation. A grid column is identified as a convective column if a) the reflectivity at any height is greater than 50 dBZ, or b) if the reflectivity at –10°C height or above is greater than 30 dBZ, or c) if there is one or more lighting flashes in the bin location. Temperature soundings are obtained from the NCEP RUC 20km model analysis. The computation of the two VPRs is the same as for the volume mean VPR except that the reflectivity data are now divided into two groups, one is for convective and another is for stratiform regions. Examples of convective and stratiform VPRs are shown in section 2.2.

2.2 Case Study

The Texas squall line event of 1 June 2005 was used to calculate and to examine the VPR characteristics of different precipitation types (convective and stratiform). Figure 3 shows composite reflectivity (left column), precipitation type (center

column), and a vertical cross section (right column) as a large convective complex passed over the KEWX (Austin/San Antonio, Texas) WSR-88D radar site beginning at 0900 UTC and ending at 1200 UTC. At the time of 0900 UTC (Fig.3a), a bow-shaped convective line oriented in west-east direction was centered over the KEWX radar. The automated precipitation-typing algorithm properly identified convective storms cells (Fig.3b). The vertical cross section running southwest – northeast through the radar site shows a line of convective storm cells (Fig.3c). As the convective line moved south, a broad region of stratiform cloud and precipitation encompassed KEWX site by 1000 UTC (Fig.3d). The stratiform region was characterized by horizontal uniformity with a distinct 'bright-band' layer centered around 3.4km above mean sea level (MSL) (Fig.3f). By 1200 UTC, the convective system had moved to the gulf coast with no subsequent development of convective precipitation in the vicinity of the KEWX radar (Figs.3j and 3k).

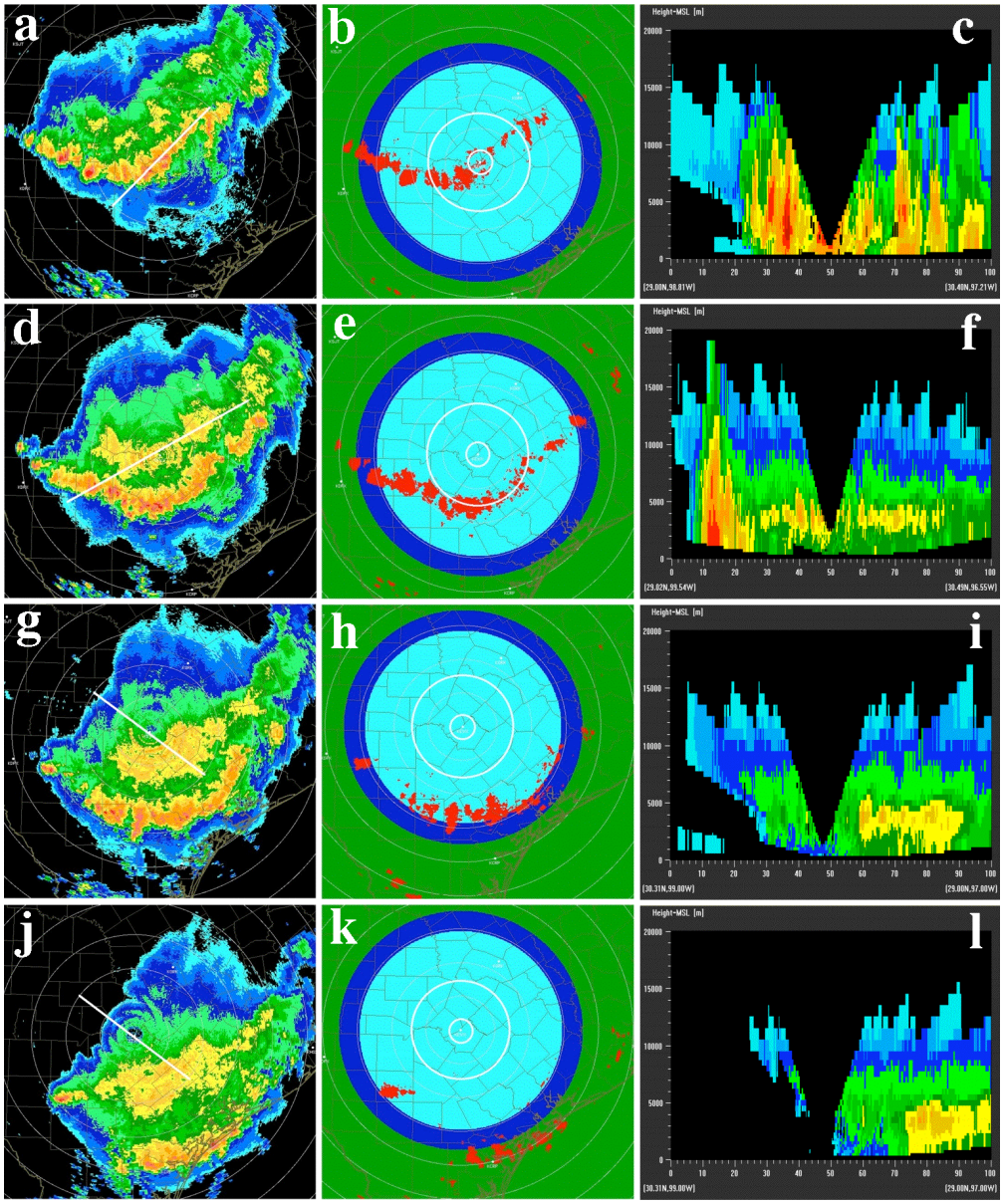

Fig. 3 Composite reflectivity (left), precipitation type (middle), and vertical cross section of reflectivity (right) fields derived from KEWX (Austin, TX) radar observations at 0902 (1st row), 1000 (2nd row), 1104 (3rd row) and 1202Z (4th row), respectively, on 1 June 2005. The thin white rings in the left and middle columns are range rings for

every 35 miles. The color red in precipitation type fields indicates convective regions and other colors indicate stratiform regions (different colors mean different beam height zones). The bold white lines in the composite reflectivity images depict where the vertical cross sections (in the right panels) were taken. The bold white circles indicate the annular region where vertical profiles of reflectivity were computed.

Figure 4 shows hourly mean vertical profiles of reflectivity derived from convective and stratiform regions, respectively. The hourly mean VPRs were obtained by averaging the volume mean VPRs from each individual volume scans within a given hour. The mean volume scan VPRs were calculated using a volume scan of reflectivity observations within a pre-specified annular region (see section 2.1). The two bold white circles in the precipitation type fields (Figs.3b, 3e, 3h, and 3k) show the inner and outer boundaries of the annulus region (20 and 80km in the present study), respectively. A convective VPR was not obtained during 1100-1200UTC (Fig.4e) because of insufficient convective precipitation identifications in the pre-specified annular region (Figs.3h and 3k).

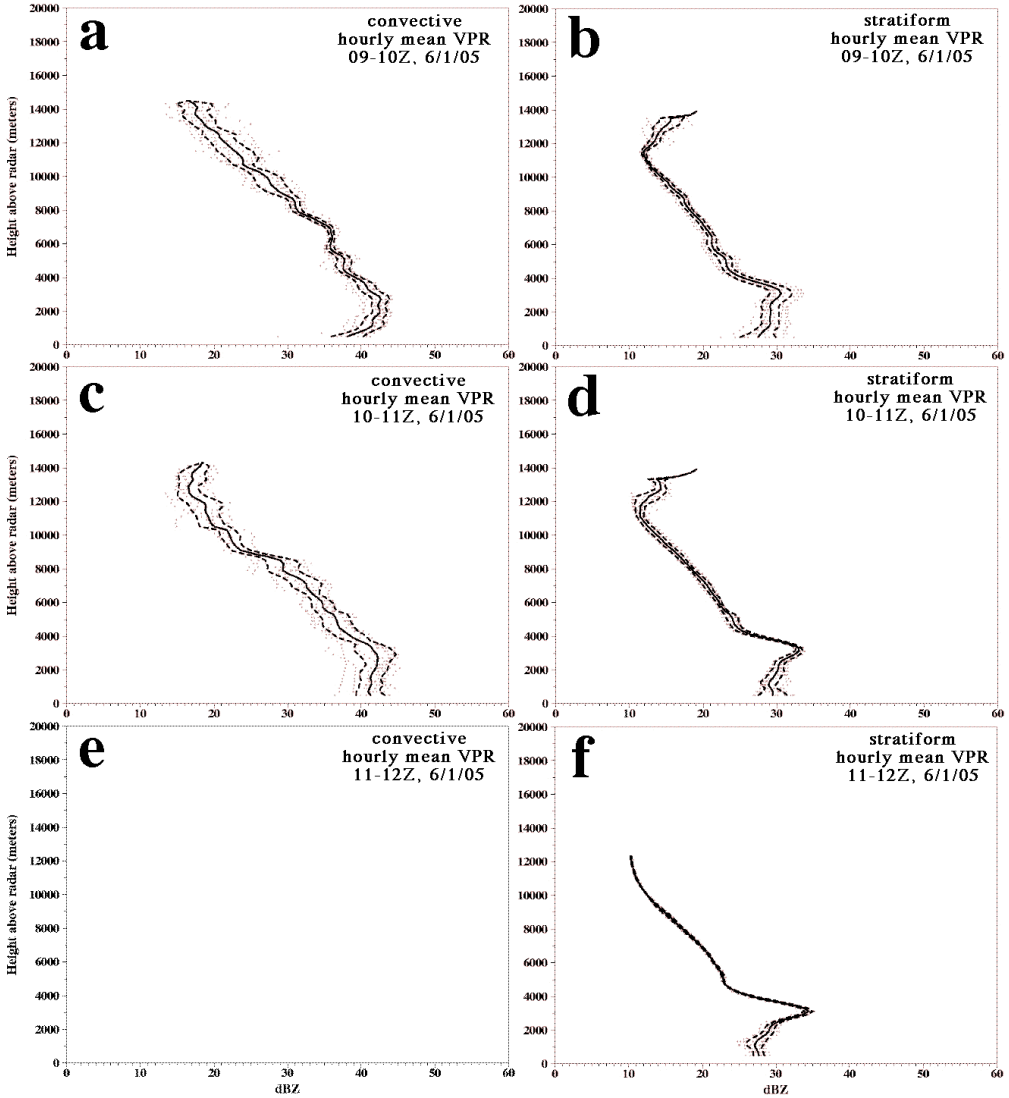

Fig. 4 Hourly mean VPRs derived for convective (left) and stratiform (right) precipitation regions at three consecutive time periods on 1 June 2005: 0900-1000UTC (top row), 1000-100UTC (middle row) and 1100-1200UTC (bottom row). The brown dots represent mean VPRs derived from each individual volume scans within the hour, the black line represents the average of the mean VPRs from individual volume scans, and the dashed lines indicate +/- one standard deviation of the individual volume mean VPRs in the hour.

A comparison between the stratiform and convective VPRs yields significant differences. For example, there exists a considerably larger standard deviation in the vertical structure of convective VPR than in that of stratiform VPR (compare Figs.4a and 4c versus Figs.4b, 4d). The large standard deviation is likely a reflection of the variance in intensity, depth, and horizontal extent of a convective storms reflectivity structure. The magnitude of this variance, as captured in the single volume VPR, is dependent up on the life cycle stage as well as the near storm environment (instability, moisture availability, etc). Even with a single storm cell, the vertical and horizontal distributions of reflectivity vary from the center (core) to the edges of the storm cell. In Fig.3c, the vertical cross section intercepted a series of individual storm cells. Even though all the storms showed characteristics of upright cores, the depths and heights of the cores varied from cell to cell (Fig.3c). In addition to the spatial inhomogeneity, convective storms have a distinct life cycle evolution, which occurs on the order of 10s of minutes (pulse storms) to hours (in the case of supercells). All of these factors contribute to variance among individual volume VPRs, which then contributes to the large standard deviation.

In Fig.4 the brown dots are VPRs derived from each individual volume scans. The scattering of the brown dots in Figs.4a and 4c indicates large changes in convective VPR during the hour. The changes are much smaller in stratiform VPR, especially after 10Z (Figs.4d and 4f). The hourly mean convective VPR during 0900-1000UTC (Fig.4a) is very similar to the VPR during 1000-1100UTC, except for the lowest 1km where reflectivity decreases towards the ground. This decrease is likely due to the evaporation of rain particles below the cloud base where the atmosphere was initially dry (Fig.5a). The evaporation become less significant as the rainfall moistened the lower atmosphere (Fig.5b) during the later stages of the event.

While the hourly mean stratiform VPR during 0900-1000UTC showed some scattering (Fig.4b), this was due to the inclusion of the outer edges of the convective storms within the annulus. These regions were identified as 'stratiform' because of the strict intensity requirements for convective identification. Nevertheless, the sharp gradient between 3.2 and 4.5 km above radar level shows a very distinct signal of bright-band layer that does not exist in the convective VPR (Fig.2a). Since the KEWX radar is 218 m above MSL, the maximum reflectivity level (3.2km above radar level) coincided very well with the bright-band layer (3.4km above MSL) in the vertical cross section (Fig.4f). During 1000-1100UTC, the majority of the annular sampling region (Fig.4e and 4h) was in stratiform precipitation. As a result, the hourly mean stratiform VPR became better defined in comparison to the previous hour with the scattering among the single volume scan VPRs becoming smaller. The bright-band layer (Fig.4d) was better sampled by the radar than in the previous hour. After 1100UTC, the whole annular area was filled with stratiform echoes. The stratiform clouds and precipitation were quasi-stationary and horizontally homogeneous, with the volume scan mean VPR changed very little during the hour. The bright-band signature was further defined in the hourly mean VPR because of the better sampling and lack of contamination from the outer edges of convective regions.

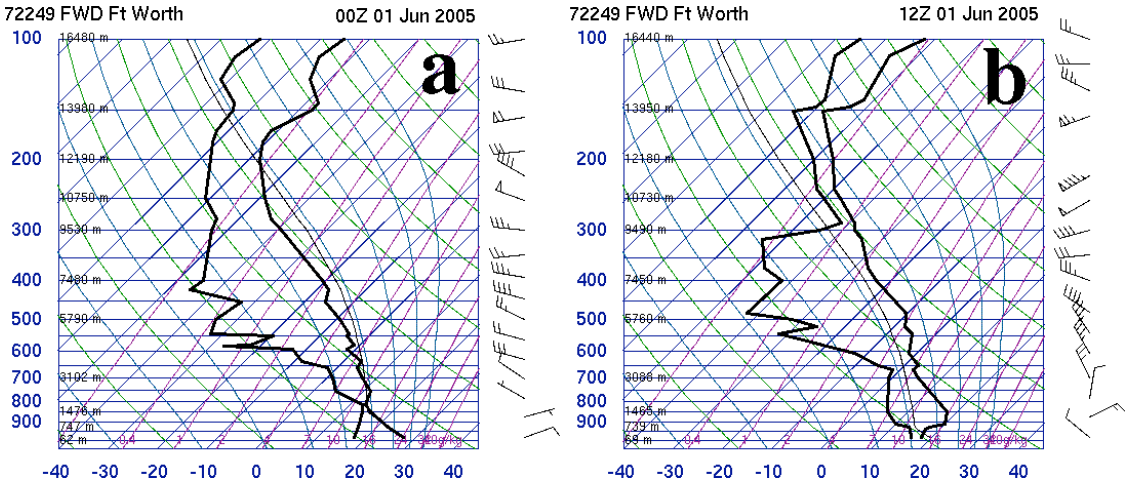

Fig. 5 Skew-T plots of the sounding observations at the Ft. Worth, Texas at 0000UTC (*a*) and 1200UTC (*b*) on 1 June 2005.

3 Gap Filling in the 3D Mosaic Using VPR

The hourly mean convective and stratiform VPRs are infused in the 3D reflectivity mosaic analysis for gap filling the data voids at the lower levels. There are four steps in the gap-filling procedure:

1) for each grid column, searching from the bottom up until a non-missing value, Z_1 is found; Suppose that the height where Z_1 was found is h_1 (Fig. 6a);

2) computing difference between Z_1 and the hourly mean VPR reflectivity, $\overline{Z}[h_1]$, at the height of h_1 (Fig. 6b), i.e.,

$$\Delta Z_1 = Z_1 - \overline{Z}[h_1] \quad (1)$$

3) for each grid cell below the height of h_1, find the mean VPR reflectivity value $\overline{Z}[h_2]$ at the same height of the grid cell, h_2 (Fig. 6b);

4) filling in the grid cell with a new reflectivity value, Z_2, which is determined by the following formula (Fig. 6c):

$$Z_2 = \overline{Z}[h_2] + \Delta Z_1 \quad (2)$$

Note that the mean VPR used in the procedure should be consistent with the precipitation type in the grid column. If the precipitation type in the grid column is convective, then the hourly mean convective VPR is used to find $\overline{Z}[h_1]$ and $\overline{Z}[h_2]$. Otherwise a stratiform VPR is used.

Figure 7a shows a vertical cross section from a 3D reflectivity analysis grid using KDYX radar observation at 0400UTC on 1 June 2005. The vertical cross section was taken along a line ~170km to the southwest of the radar (see the white line in Fig.7d). At this range, the bottom of the lowest radar beam is ~1.9km above the radar level (Fig.1), resulting in data voids at the lower levels of the analysis domain (Figs. 7a and 7d). After gap filling utilizing the hourly mean VPRs, the data voids were successfully filled in. Using the VPRs, the coverage was extended down to the lower levels (Fig.7b) with the storm distributions on the 1.25km MSL horizontal cross section more physically realistic than without the gap filling (compare Figs. 7d and 7e). A vertical and a horizontal cross-section from the 3D reflectivity analysis grid were compared to the KSJT radar (which was not included in the 3D mosaic grid) at the same time to validate the gap-filling results. The vertical cross-section was taken along a line very close to KSJT radar (~30km northeast of the radar, Fig. 7f), to obtain low-level vertical detail for comparison and validation (Fig. 7c). The vertical structure in the gap-filled reflectivity analysis grid (Fig. 7b) was consistent with the observed, even though the observed had more detail given the close proximity to the radar (Figs. 7c&7f). The horizontal storm structure after gap filling (Fig. 7e) compares very well with the observations (Fig.7f), indicating that the VPRs used in the gap filling was representative of the storm structure.

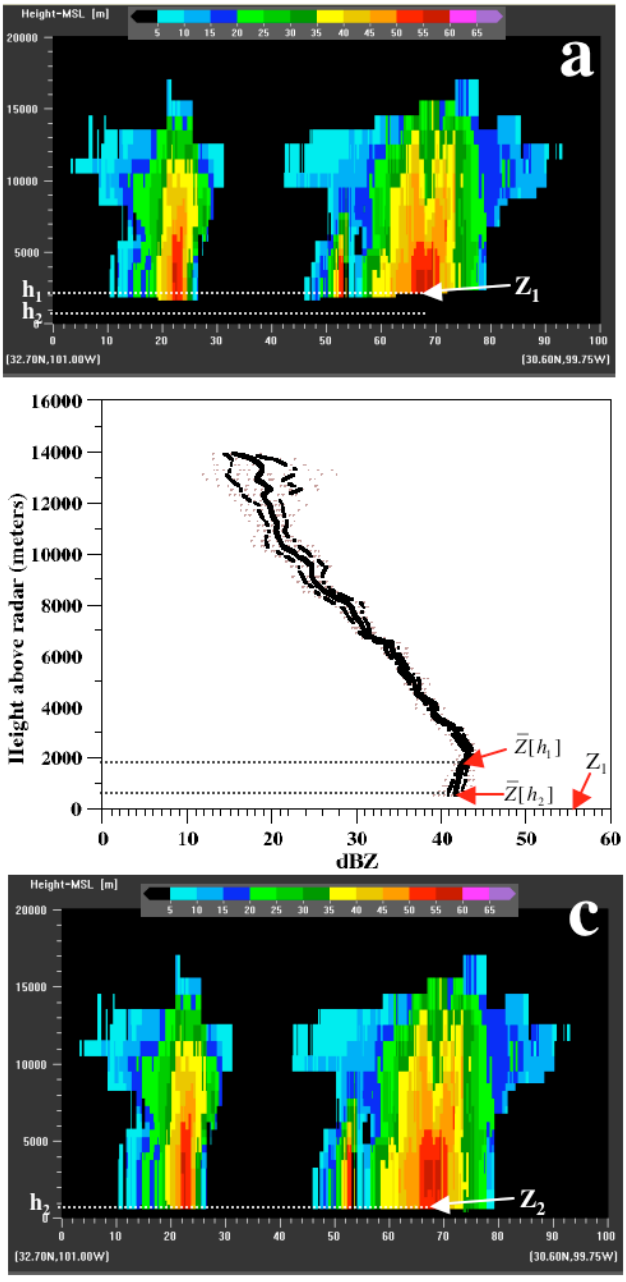

Fig. 6 An example hourly mean VPR (*b*), a vertical cross section of reflectivity before (*a*) and after (*c*) gap-filling using the mean VPR. In panel *b*, the solid black line is the mean VPR, the long dashed lines

are +/- one standard deviation of the individual volume mean VPRs in the hour.

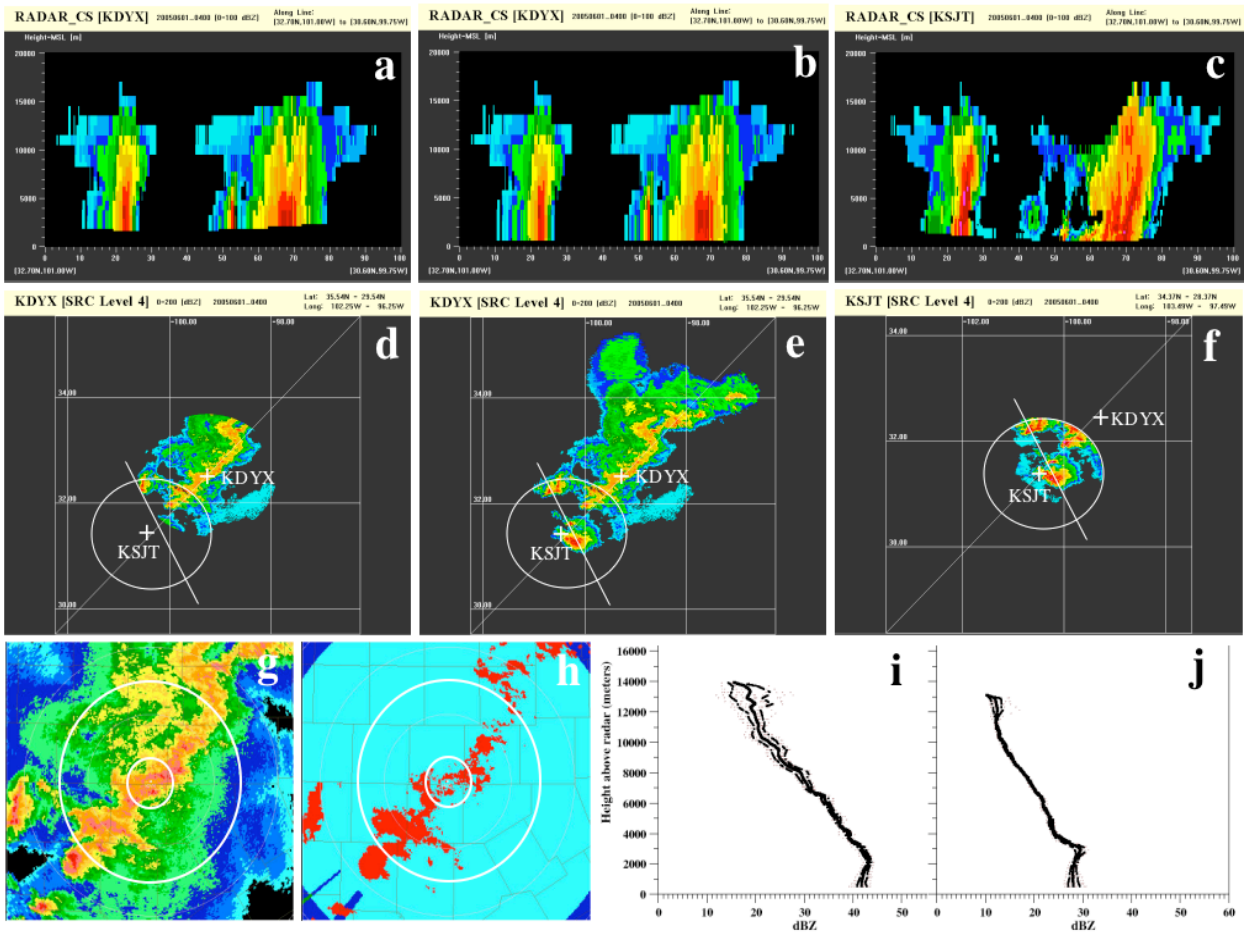

Fig. 7 A vertical cross section of reflectivity from KDYX radar observations at 04:00UTC on 1 June 2005 before (*a*) and after (*b*) gap-filling using the hourly mean convective (*i*) and stratiform (*j*) VPR. The same vertical cross-section taken from KSJT radar grid is shown in panel *c* for validation. The vertical cross-sections were taken along the lines shown in panels' *d*, *e*, and *f*, respectively. A horizontal cross section on 1.25km above MSL before (*d*) and after the gap-filling (*e*) from the KDYX reflectivity grid show that the gap-filling successfully filled in the data voids and provided a more complete depiction of the storms at this level. The gap-filled reflectivity structure (*e*) is physically sound and consistent with the observations from a nearby radar KSJT (*f*). Note that the white circles in panels *d*, *e*, and *f* indicate the KSJT coverage at the 1.25km MSL. The composite reflectivity (*g*) and the precipitation flag (*h*) fields show the distribution of precipitation echoes in regions (bounded by the two white circles) where the hourly mean VPR were derived.

4 SUMMARY

A new gap-filling technique has been developed which uses vertical profiles of reflectivity (VPRs) to fill in data voids at the lower levels in the 3D reflectivity mosaic grid. The data voids were a result of the earth's curvature and positive scan elevation angles of radar. Characteristics of VPRs in convective and stratiform precipitation were investigated. It was found that volume mean convective VPRs vary significantly from volume scan to volume scan due to the fact that convective storm structure change significantly both in space and in time. The volume mean stratiform VPRs, however, show smaller changes than the convective VPRs from volume scan to volume scan. Using the VPRs, reflectivity of the lowest radar beam was extrapolated downward to fill in gaps between the lowest radar beam and the surface. The gap-filling resulted in a more physically realistic storm coverage and structure in the lower levels of the 3D mosaic analysis. Further, the gap-filled storm structure showed good consistency with independent radar observations. The new 3D mosaic

analysis with the gap-filling will provide better reflectivity data for assimilation in NWP models and will potentially improve quantitative precipitation estimates as well as more representative severe storm parameters.

Acknowledgements

Major funding for this research was provided under the Federal Aviation Administration (FAA) Aviation Weather Research Program Advanced Weather Radar Technologies Product Development Team MOU and partial funding was provided under NOAA-University of Oklahoma Cooperative Agreement #NA17RJ1227, U.S. Department of Commerce.

This research is in response to requirements and funding by the Federal Aviation Administration (FAA). The views expressed are those of the authors and do not necessarily represent the official policy or position of the FAA.

References

Andrieu, H., and J. D. Creutin, 1995: Identification of vertical profiles of radar reflectivity for hydrological applications using an inverse method. Part I: Formulation. *J. Appl. Meteor.,* **34,** 225 – 239.

——, G. Delrieu, and J. D. Creutin, 1995: Identification of vertical profiles of radar reflectivity for hydrological applications using an inverse method. Part II: Sensitivity analysis and case study. *J. Appl. Meteor.*, **34,** 240–259.

Berne, A., G. Delrieu, H. Andrieu, and J.-D. Creutin, 2004: Influence of vertical profile of reflectivity on radar-estimated rain rates at short time steps. J. hydromet., 5, 296-310.

Joss, J., and A. Waldvogel, 1990: Precipitation measurement and hydrology. *Proc. Battan Memorial and 40th Anniversary Radar Meteor. Conf., Boston, MA,* Amer. Meteor. Soc., 577–606.

Kitchen, M., R. Brown, and A. G. Davies, 1994: Real-time correction of weather radar data for the effects of bright band, range and orographic growth in widespread precipitation. *Quart. J. Roy. Meteor. Soc.,* **120,** 1231–1254.

Koistinen, J. 1991: Operational correction of radar rainfall errors due to the vertical reflectivity profile. *Preprints, 25th Int. Conf. On Radar Meteorology,* Paris, France, Amer. Meteor. Soc., 91–96.

Pellarin, T., G. Delrieu, G.-M. Saulnier, H. Andrieu, B. Vignal, and J.-D. Creutin, 2002: Hydrological visibility of weather radar systems operating in mountainous: case study for the Ardeche catchment (France). J. hydromet., 3, 539-555.

Seo, D.-J., J. Breidenbach, R. Fulton, D. Miller, and T. O'Bannon, 2000: Real-time adjustment of range-dependent biases in WSR-88D rainfall estimates due to nonuniform vertical profile of reflectivity. *J. Hydrometeor.,* **1,** 222–240.

Vignal, B., and W. F. Krajewski, 2001: Comprehensive large sample evaluation of two methods to correct range-dependent error for WSR-88D rainfall estimates. J. Hydrometeor., 2, 490–504.

——, H. Andrieu, and J. D. Creutin, 1999: Identification of vertical profiles of reflectivity from volume scan radar data. *J. Appl. Meteor.*, 38, 1214–1228.

Zawadzki, I. 1984: Factors affecting the precision of radar measurements of rain. *Preprints, 22nd international conference on radar meteorology.* AMS. 251-256.